The Dolaflexin-based Antibody–Drug Conjugate XMT-1536 Targets the Solid Tumor Lineage Antigen SLC34A2/NaPi2b

Natalya D. Bodyak, Rebecca Mosher, Aleksandr V. Yurkovetskiy, Mao Yin, Charlie Bu, Patrick R. Conlon, Damon R. Demady, Michael J. DeVit, Dmitry R. Gumerov, Venu R. Gurijala, Winnie Lee, Dennis McGillicuddy, Peter U. Park, Laura L. Poling, Marina Protopova, LiuLiang Qin, Cheri A. Stevenson, Elena Ter-Ovanesyan, Alex Uttard, Dongmei Xiao, Jian Xu, Ling Xu, Donald A. Bergstrom, and Timothy B. Lowinger

ABSTRACT

Target selection for antibody–drug conjugates (ADC) frequently focuses on identifying antigens with differential expression in tumor and normal tissue, to mitigate the risk of on-target toxicity. However, this strategy restricts the possible target space. SLC34A2/NaPi2b is a sodium phosphate transporter expressed in a variety of human tumors including lung and ovarian carcinoma, as well as the normal tissues from which these tumors arise. Previous clinical trials with a NaPi2b targeting MMAE-ADCs have shown objective durable responses. However, the protein-based biomarker assay developed for use in that study was unable to discern a statistically significant relationship between NaPi2b protein expression and the probability of response. XMT-1536 is a NaPi2b targeting ADC comprised of a unique humanized antibody conjugated with 10–15 auristatin F- hydroxypropylamide (AF-HPA) payload molecules via the Dolaflexin platform. AF-HPA is a cell-permeable, antimitotic compound that is slowly metabolized intratumorally to an active, very low-permeable metabolite, auristatin F (AF), resulting in controlled bystander killing. We describe the preclinical *in vitro* and *in vivo* antitumor effects of XMT-1536 in models of ovarian and lung adenocarcinoma. Pharmacokinetic analysis showed approximately proportional increases in exposure in rat and monkey. Systemic free AF-HPA and AF concentrations were observed to be low in all animal species. Finally, we describe a unique IHC reagent, generated from a chimeric construct of the therapeutic antibody, that was used to derive a target expression and efficacy relationship in a series of ovarian primary xenograft cancer models.

Introduction

Antibody–drug conjugates (ADC) enable the tumor-targeted delivery of cytotoxic agents. This therapeutic modality reduces the systemic toxicity associated with potent chemotherapeutic agents while enhancing the antitumor activity (1, 2).

Of the seven FDA-approved ADCs, four target lineage-specific hematologic antigens that are not markedly differentially expressed in neoplastic versus nonneoplastic cells. CD30 is expressed in activated T and B cells (3, 4); brentuximab-vedotin, an ADC targeting CD30, is approved for the treatment of tumors arising from these cell populations, including Hodgkin lymphoma and systemic anaplastic large cell lymphoma (2, 5, 6). Inotuzumab ozogamicin targets CD22, a B-cell lineage antigen, and is approved for B-cell precursor acute lymphoblastic leukemia (7). Gentuzumab ozogamicin targets CD33, a myeloid lineage antigen, and is approved for acute myeloid leukemia (8). Polatuzumab vedotin targets CD79b, an antigen expressed in B cells and B-cell lymphoma (9).

In contrast, the strategy for solid tumor ADCs generally had been to focus on targets that are "overexpressed" in tumors versus normal tissue to avoid toxicity associated with antibody-mediated delivery of cytotoxin to normal tissues. For example, two approved ADCs for solid tumors, trastuzumab emtansine (2) and trastuzumab deruxtecan (10) target ERBB2 (HER2), which is significantly overexpressed in a subset of breast cancer versus normal tissue.

Recent clinical studies with other targets in solid tumors have yielded two approved entities, Nectin-4-targeted enfortumab vedotin (11) and Trop-2–targeted sacituzumab govitecan (12). Nectin-4 is expressed in normal skin, and while rash and alopecia were described in the clinical study, they were not the most prominent adverse effects. Trop-2 expression has also been described in normal tissues (13), but here the most prominent clinical adverse effects were similar to irinotecan, including neutropenia and diarrhea. Thus, it appears that targeting proteins expressed in normal epithelial and tumor tissue with ADCs is possible and that we could refine our strategies both for ADC target selection and technology to expand the target space (14, 15).

NaPi2b is a transmembrane sodium phosphate transporter protein encoded by the SLC34A2 gene and is expressed in both tumor and normal tissue. Expression by protein or RNA methods has been described in nonsquamous non–small cell lung carcinoma, nonmucinous ovarian carcinoma, and papillary thyroid carcinoma; normal tissue expression has been reported in lung, bronchus, and kidney (16). In normal lung tissue, NaPi2b plays a role in phosphate transport, and mutations in SLC34A2 are associated with pulmonary and testicular microlithiasis (17).

Lifastuzumab vedotin, an ADC that targets NaPi2b and utilizes the vcMMAE ADC linker-payload, has been evaluated in phase I and II

Mersana Therapeutics, Inc., Cambridge, Massachusetts.

Note: Supplementary data for this article are available at Molecular Cancer Therapeutics Online (http://mct.aacrjournals.org/).

Corresponding Author: Timothy B. Lowinger, Mersana Therapeutics, Inc., 840 Memorial Drive, Cambridge, MA 02139. E-mail: tlowinger@mersana.com

Mol Cancer Ther 2021;20:896–905

doi: 10.1158/1535-7163.MCT-20-0183

clinical trials (18, 19). Lifastuzumab vedotin achieved a 34% overall response rate in the ITT population at the recommended phase II dose in patients with heavily pretreated platinum-resistant ovarian cancer, but it was not statistically superior to liposomal doxorubicin in a randomized phase II trial. In the biomarker analysis, using the anti-NaPi2b (10H1) mouse mAb IHC assay developed for this trial, most patients showed strong NaPi2b protein expression, precluding development of an expression/efficacy relationship. However, a qRT-PCR RNA expression method chosen to increase the analytic dynamic range showed a trend between NaPi2b expression and efficacy in the phase II subgroup analysis.

We hypothesized that NaPi2b would be a target well-suited to the Dolaflexin ADC technology (20). This polymer-based platform has several advantages over conventional ADC platforms. The Dolaflexin platform yields high drug–antibody ratio (DAR) ADCs with an average of 10–15 AF-HPA payload molecules per antibody, as opposed to 3–4 in many conventional ADCs. AF-HPA is cell permeable and can diffuse to adjacent cells to cause bystander cytotoxicity. AF-HPA is also metabolized intratumorally to an active metabolite, auristatin F (AF), that is essentially cell impermeable and is not a substrate for the PgP drug efflux pump. The resulting controlled bystander effect leads to efficacy in tumors with heterogeneous antigen expression and improved systemic tolerability (21). Furthermore, higher DAR ADCs might be efficacious in tumors types with a range of antigen expression.

XMT-1536 is an ADC targeting NaPi2b and is comprised of a unique humanized anti-NaPi2b antibody conjugated to Dolaflexin (22). Consistent with the higher DAR, XMT-1536 showed greater antitumor activity than lifastuzumab-vedotin in both ovarian cancer and non–small cell lung cancer (NSCLC) primary patient-derived xenograft models (PDX). Evaluation of XMT-1536 in toxicology studies in rat and cynomolgus monkey established a tolerability profile with a notable absence of neutropenia, the dose-limiting toxicity observed for lifastuzumab vedotin.

These data support clinical evaluation of XMT-1536 for the treatment of patients with NaPi2b-expressing tumors and the general concept of exploring lineage markers as targets for ADCs.

Materials and Methods

IHC

IHC was performed at QualTek Molecular Laboratories using an automated TechMate 500 or TechMate 1000 (BioTek Solutions/Ventana Medical Systems) platform.

Four-micron–thick sections were cut, dewaxed, and rehydrated through xylene and a series of alcohols. Slides were antigen retrieved in a standard steamer using BioGenex AR-10 retrieval solution. On the TechMate platform, further retrieval was performed with Proteinase K (DAKO). Following serum blocking, the primary antibody, comprised of a human-rabbit chimera of XMT-1535 (the antibody component of XMT-1536, described below), was applied for 30 minutes at room temperature, secondary antibody for 25 minutes at room temperature, then endogenous peroxidase block and nonbiotin polymer-based detection (rabbit Polink-2 Plus detection system, GBI) was used and finally a brief hematoxylin counterstaining

Tissues were either formalin-fixed, paraffin embedded (FFPE) xenograft tumors or banked human tumors obtained from Conversant BioSciences. Slides were scanned on an Aperio slide scanning system and images saved as 20× TIFF files. Representative fields were obtained from TIFF files using Windows Snipping Tool.

ADC synthesis

The targeting antibody in XMT-1536, XMT-1535, also known as Rebmab200, is a humanized version of the MX35 murine antibody that was generated from mice immunized with a mixture of four ovarian cancer cell lines (23) and that was later shown to recognize NaPi2b, the sodium-dependent phosphate transport protein 2b (NaPi2b) encoded by the *SLC34A2* gene (24). The humanization strategy and characterization of XMT-1535 (Rebmab200) has been described previously (25, 26). Antibody material used in this work was material described in ref. 23 or a subsequent batch manufactured at a contract research organization. The antibody sequence is described in patent application US 2017/0266311A1 and referred to as XMT-1535 (27).

The structure and generalized process for production of Dolaflexin ADCs is shown in Supplementary Fig. S2. For the production of XMT-1536, the antibody XMT-1535 (350 mg, 9.97 mg/mL in sodium acetate, pH 5.5 buffer) was diluted with bioconjugation buffer (50 mmol/L triethyl ammonium acetate, 1 mmol/L EDTA, pH = 7.0) to provide a 5 mg/mL solution, to which was added 1.73 mg of TCEP (345 μL, 5 mg/mL, 2.5 equivalent) dropwise, and the resulting reaction mixture was stirred for 90 minutes at 37°C. In a separate flask, 315 mg (on a dry basis) of Dolaflexin (15.37 mL, 20.5 mg/mL, 0.9/1 wt/wt) was diluted with 16.13 mL of bioconjugation buffer to provide a 10 mg/mL solution, and the pH was adjusted to 6.5 with 1 N $NaHCO_3$. After 90 minutes, the reduced XMT-1535 solution was added by peristaltic pump to the vigorously stirred Dolaflexin solution over approximately 15–20 minutes. The reaction mixture was stirred at room temperature for an additional 45 minutes and excess maleimide was quenched by the addition of 14.2 mg of L-cysteine (dissolved in 2 mL conjugation buffer, 50 molar equiv.). After stirring for an additional 30 minutes, the reaction mixture was adjusted to pH 5.8 with 1 mol/L acetic acid and filtered through a 0.2-μm filter. The crude ADC was purified by SCX-HPLC (Thermo Fisher Life Technologies, POROS GoPure HS 50-μm resin prepacked column 1.2 cm D x 20 cm L, mobile phase A 50 mmol/L sodium acetate pH = 5.8, Mobile phase B 50 mmol/L sodium acetate 1 mol/L NaCl, with a step gradient 3% B and 9.5% B at 4 mL/minute in 100 minutes). Fractions corresponding to the desired product were pooled and concentrated by tangential flow filtration using a 10 kDa MWCO membrane, providing XMT-1535-Dolaflexin, now referred to as XMT-1536.

The IgG-Dolaflexin, nonbinding ADC was constructed using the preceding protocol, with Rituxan (rituximab; Biogen & Genentech) as the antibody.

Lifastuzumab-vedotin was made according to the method described previously (16). DAR of these preparations was either 3.1 or 4.1.

Peptide binding

Cyclic NaPi2b peptide was generated and used to coat 96-well high binding clear ELISA plates (Corning, 3369) at 1 μg/mL in sodium carbonate buffer, pH 9, to a total volume of 100 μL per well. After a 2-hour incubation, plates were washed four times with 100 μL per well TBS-Tween 20, blocked with 3% BSA in TBS-Tween 20 (100 μL per well) for 1 hour, and washed again. Test articles (run in duplicate in three assay runs) were added to the wells at a dose concentration range from 100 nmol/L to 0.002 nmol/L using an 8-point 3-fold serial dilution in TBS-Tween 20 buffer at 100 μL per well. Plates were incubated for 1 hour at room temperature with rocking then washed as above. Peroxidase-conjugated AffiniPure Goat Anti-Human IgG F(ab')2 fragment specific secondary antibody was used at 5,000x in TBS-Tween 20 buffer at 100 μL per well. Plates were again incubated for 1 hour with rocking followed by wash as above. TMB substrate was added at 50 μL per well and incubated until color appeared and then

the reaction was quenched with 50 μL of 0.2N H_2SO_4. The optical density (OD) was measured at 450 nm with a SpectraMax M5 microplate reader (Molecular Devices). The K_d was calculated with GraphPad Prism software (GraphPad Software Inc.) by nonlinear regression using the one site-specific binding model.

Cell binding

OVCAR3 ovarian carcinoma cells (ATCC) were grown to approximately 90% confluency and released from the plate surface using Accutase. Cells were then washed once with ice-cold media, resuspended in ice-cold media containing 6% goat serum, seeded at a density of 50,000 cells per well and incubated on ice for 3 hours with a range of XMT-1536 or XMT-1535 concentrations (0.01–500 nmol/L, $n = 5$). The cells were washed three times with 100 μL ice-cold PBS, resuspended in 100 μL media with 2% goat serum and 5 μg/mL of Alexa Fluor 647-labeled goat anti-human IgG, and incubated in the dark on ice for 1 hour. The cells were washed three times with 100 μL ice-cold PBS and resuspended in 100 μL of ice-cold PBS with 1% paraformaldehyde. The median fluorescence value for each treatment was determined from 5,000 cells quantified on a MACSQuant flow cytometer (Miltenyi Biotec). The K_d was calculated with GraphPad Prism software (GraphPad Software Inc.) by nonlinear regression using the one site-specific binding model.

Cell identity and negative *Mycoplasma* status was confirmed by CellCheck 9 plus method at multiple passages (IDEXX BioResearch).

ADC internalization

OVCAR3 cells were grown on chambered cover glass and incubated with ADC for 1 hour on ice. Cells were then washed with ice-cold PBS and incubated on ice with a goat anti-human IgG monovalent Fab fragment conjugated to Alexa Fluor -647 for 1 hour. After washing, the cells were transferred to a 37°C incubator to allow internalization for 0, 1, 3, 6, and 24 hours. The cells were then placed on ice, washed with ice-cold PBS, and incubated for 5 minutes with Cellmask Orange to visualize the plasma membranes and Lysosensor Green DND-189 to show colocalization with the lysosomes. After washing, the cells were imaged on a Zeiss Axio Vert.A1 FL inverted microscope.

In vitro cytotoxicity

OVCAR3 cells were grown in RPMI1640 media supplemented with 20% FBS and 1% penicillin/streptomycin, seeded at a density of 5,000 cells per well in 100 μL of growth media in a 96-well, white flat-bottom plate. Following overnight incubation, the media was replaced with 100 μL of fresh media containing the test compounds at a 3-fold titration up to 33 nmol/L. The treated cells were incubated for 96 hours at 37°C in the presence of 5% CO_2. Cell viability was determined using The CellTiter-Glo Luminescent Cell Viability Assay and luminescence was quantified with SpectraMax M5 microplate reader (Molecular Devices). Cell viability was normalized to untreated control and expressed as a percentage. IC_{50} values were calculated with GraphPad Prism software (GraphPad Software Inc.) using 4-parameter, variable slope, dose–response curve fitting algorithm. Cell line studies were performed as $n = 3$ with each treatment.

Effect on cell cycle

OVCAR3 cells were treated with XMT-1536 ranging from 0 to 1 nmol/L and in some cases 30 nmol/L Bafilomycin A for 24 hours. The amount of nuclear DNA in each cell was quantified in 5,000 cells for each treatment by a MACSQuant flow cytometer (Miltenyi Biotec) using propidium iodide. The percentage of arrested cells was determined by dividing the number of cells in G_2–M phase by the total number of cells and multiplying by 100.

In vivo studies

All procedures in animals were performed in compliance with the Animal Welfare Act, the Guide for the Care and Use of Laboratory Animals, and the Office of Laboratory Animal Welfare. Protocols were reviewed and approved by the Institutional Animal Care and Use Committees of the relevant facility.

In vivo efficacy

OVCAR3 model

Xenografts were initiated with OVCAR3 human ovarian carcinoma fragment (~1 mm^3) implanted subcutaneously in the right flank of 8-week-old female CB17-severe combined immunodeficiency (SCID) mice (Charles River Discovery Services North Carolina). Animals were randomized into treatment groups ($n = 10$) when the tumor target volume reached 100–150 mm^3. Test articles were administered intravenously via tail vein injection. Mice received a single dose of either saline vehicle; XMT-1535 at 3 mg/kg; XMT-1536 (DAR 12.4) at 3 mg/kg; IgG1-Dolaflexin (DAR 18.1) at 3 mg/kg, or lifastuzumab vedotin (DAR 4.1) at 3 mg/kg. Tumors were measured twice per week. The study endpoint was tumor volume (TV) of 1000 mm^3 or day 57, whichever came first. A partial response (PR) was defined as a tumor volume that was 50% or less of its day 1 volume for three consecutive measurements throughout the study, and equal to or greater than 13.5 mm^3 for one or more of these three measurements. In a complete response (CR), the tumor volume was less than 13.5 mm^3 for three consecutive measurements during the study. An animal with a CR at the termination of a study was additionally classified as a tumor-free survivor (TFS). The log rank (Mantel–Cox) and Gehan–Breslow–Wilcoxon tests were employed to assess the significance of the difference between the overall survival experiences of two groups. For statistical analyses, two-tailed tests were conducted at significance level $P = 0.05$.

Primary lung cancer xenografts

Nu/Nu 7-week-old female mice were implanted with human NSCLC models CTG-0178 (moderately differentiated lung adenocarcinoma), CTG-0852 (poorly differentiated lung adenocarcinoma), and CTG-0860 (poorly differentiated lung adenocarcinoma), expressing NaPi2b mRNA (Champions Oncology). After the tumors reached 1–1.5 cm^3, they were harvested and the tumor fragments of approximately 5 × 5 × 5 mm^3 were implanted subcutaneously in study mice. Animals were randomized among the treatment groups ($n = 8$) when the tumor volumes reached approximately 100–300 mm^3, and treated with saline vehicle, lifastuzumab vedotin (DAR 3.1) 3 mg/kg qwk × 3, nonspecific IgG1-Dolaflexin (DAR 16.2) 3 mg/kg qwk × 3, or XMT-1536 (DAR 13.1) 3 mg/kg qwk x 3. The study endpoint was tumor volume of 1,500 mm^3. A PR was defined as a tumor volume ≤ 30% of tumor volume at day 0 for two consecutive measurements. A CR was defined as a mouse with no palpable tumor for two consecutive measurements over a 7-day period. A TFS was a CR that persisted until study completion. Statistical analyses were performed using one-way ANOVA followed by Dunnett multiple comparison tests.

Primary ovarian cancer xenografts

Immunocompromised female mice (either Athymic Nude or CB-17 SCID, 6–12-week-old) were implanted with human primary xenograft tumors representing human ovarian or fallopian cancer (South Texas

Accelerated Research). These models were selected to represent a diversity of treatment exposure (12 treatment-exposed and 8 treatment-naïve), but NaPi2b expression was unknown at the time of model selection. Mice were randomized at a mean tumor volume of 125–250 mm^3. Three animals/model were dosed with XMT-1536 (DAR 12.0) at 3 mg/kg qwk × 3. The study endpoint was when tumors were 1 cm^3 or at 45 days. Tumor from an untreated animal from each model was collected at the planned endpoint. Results were reported as %T/C and are shown as median best response, calculated as the median of the greatest difference from baseline for each tumor within each model at each examined timepoint.

Toxicology and pharmacokinetics

Mouse tissue biodistribution

XMT-1536 tissue distribution was evaluated in SCID mice bearing OVCAR3 subcutaneous xenografts. Animals received a single dose of XMT-1536 (DAR 12.0) at 3.0 mg/kg. Plasma and tissues, including tumor, lung, liver, kidney, skeletal muscle and spleen, from $n = 4$/timepoint at 5 minutes, 24 hours, 72 hours, 96 hours, 7 days, and 14 days, were harvested after mice were perfused with saline. Total AF-HPA, free AF-HPA, and free AF were analyzed in plasma and tissue samples via validated LC/MS-MS methods. For clarity, free AF-HPA and free AF refer to nonconjugated AF-HPA and AF. Total AF-HPA refers to total AF-HPA after hydrolysis to release all conjugated AF-HPA in the sample. Conjugated AF-HPA can be calculated by subtracting free AF-HPA from total AF-HPA.

Rat and cynomolgus monkey toxicology

Toxicology studies were performed under Good Laboratory Practice (GLP) for Nonclinical Laboratory Studies. XMT-1536 (DAR 11.6) was administered intravenously to 9-week-old Sprague-Dawley rats and 2.4 -3.5-year old cynomolgus monkeys on days 1 and 22, with terminal necropsy at day 29/30 and recovery necropsy at day 50. Doses of 1.5 mg/kg, 3 mg/kg, and 6 mg/kg were tested in the rat, in groups of 16 male and 16 female animals (10 main study and 6 recovery). Doses of 0.75 mg/kg, 1.5 mg/kg, and 3 mg/kg were tested in the monkey, in groups of 6 male and 6 female animals (4 main and 2 recovery studies). Both studies included in-life observations, clinical pathology, gross pathology, and histopathology on a full panel of tissues, and toxicokinetics. Four different analytes, including total XMT-1535, total AF-HPA, free AF-HPA, and free AF were analyzed in the animal plasma samples through validated LC/MS-MS methods. Exposure and pharmacokinetic (PK) parameters were assessed for each analyte. PK comparisons were also made to the prior mouse plasma PK in the tissue distribution study.

Human, cynomolgus monkey and rat tissue cross-reactivity studies

XMT-1536 was applied to cryosections of normal human, monkey, and rat tissues ($n = 3$ donors per tissue for human, $n = 2$ donors per tissue for monkey and rat), at two concentrations (5 and 0.25 μg/mL). XMT-1536 was detected with a secondary antibody raised in mouse against the toxin–linker conjugate and the DAKO EnVision+kit.

Results

SLC34A2/NaPi2b is broadly expressed in epithelial ovarian cancer and lung adenocarcinoma

SLC34A2 expression was demonstrated at the protein level using an IHC assay for NaPi2b. NaPi2b IHC of a representative ovarian tumor confirmed detectable membrane expression of NaPi2b (**Fig. 1A**, and enlarged inset). In normal fallopian tube, NaPi2b expression was seen on the epithelial apical surface (**Fig. 1B**). A representative image of a lung adenocarcinoma confirmed membrane expression of NaPi2b in tumor cells (**Fig. 1C**, open arrow). In the enlarged inset, both cytoplasmic and membranous immunoreactivity are noted. The same tissue sample also demonstrated expression of NaPi2b protein on the apical surface of normal bronchial epithelium (**Fig. 1C**, solid arrow). NaPi2b expression was also detected in type 2 pneumocytes in lung parenchyma (**Fig. 1D**). The comparable expression of SLC34A2/NaPi2b in tumor and the matched normal tissue is consistent with expression being a lineage marker of the cell-of-origin, as opposed to part of the oncogenic process in these tumors.

Review of RNA-sequencing data from publicly available data sources showed levels of SLC34A2 RNA expression to be relatively higher in papillary thyroid carcinoma, lung adenocarcinoma, ovarian carcinoma and cholangiocarcinoma, in contrast to lung squamous cell carcinoma, where expression was relatively low (Supplementary Fig. S1). RNA expression also appeared relatively increased in uterine (endometrial) cancer and cholangiocarcinoma.

In vitro characterization of XMT-1536

XMT-1536 and the unconjugated antibody XMT-1535 bound to a peptide corresponding to the epitope of human NaPi2b with equivalent affinity (K_d 0.82 ± 0.28 nmol/L and 0.73 ± 0.34 nmol/L for XMT-1536 and XMT-1535 antibody, respectively). XMT-1536 showed similar affinity for the NaPi2b epitope from human, cynomolgus monkey, rat, and mouse (**Fig. 2A**). Both XMT-1536 and the unconjugated XMT-1535 antibody bound to the NaPi2b-expressing OVCAR3 ovarian cancer cell line (~66,000 NaPi2b antigens per cell) with nanomolar affinity (K_d 4.14 ± 3.08 nmol/L and 4.05 ± 2.62 nmol/L for XMT-1536 and unconjugated antibody, respectively; **Fig. 2B**). After binding, XMT-1536 internalized and trafficked to the lysosomal compartment within 3 hours (**Fig. 2C**).

In the OVCAR3 cell line, XMT-1536 was cytotoxic in a 96-hour cellular cytotoxicity assay with subnanomolar potency (EC_{50} 0.52 nmol/L expressed in AF-HPA payload equivalents), with higher potency compared with treatment with unconjugated payload (EC_{50} 0.97 nmol/L, **Fig. 2D**). In contrast, a nonbinding control Dolaflexin ADC with similar DAR to XMT-1536 (IgG1-Dolaflexin) was 30-fold less potent than XMT-1536 in cytotoxicity assays (EC_{50} 15.9 nmol/L).

Consistent with the antimitotic mechanism of action of the AF-HPA payload, treatment of OVCAR3 cells with XMT-1536 led to accumulation of cells in the G_2–M phase of the cell cycle. Cotreatment of OVCAR3 cells with Bafilomycin A (Baf.A) to block lysosomal acidification completely abrogated accumulation of cells in G_2–M (**Table 1**), indicating that internalization and lysosomal trafficking is necessary for the pharmacologic effect of XMT-1536.

XMT-1536 induced tumor regressions in a xenograft model of ovarian adenocarcinoma

XMT-1536 induced marked tumor regression of established tumors in the OVCAR3 ovarian carcinoma model when administered at a single 3 mg/kg dose (**Fig. 3A**). At this dose, there were 3 CR and 4 PR and T-C (difference in median time to endpoint for treated vs. control) was 30.9 days. XMT-1536 was well-tolerated with transient body weight loss of -6.6% at nadir (compared with −1.2% for vehicle control). Lifastuzumab-vedotin dosed once at 3 mg/kg resulted in no PRs or CRs and a T-C of 6.1 days. The nonbinding ADC IgG1-Dolaflexin and the unconjugated antibody XMT-1535 were inactive with 0/10 regressions and no significant tumor growth delay.

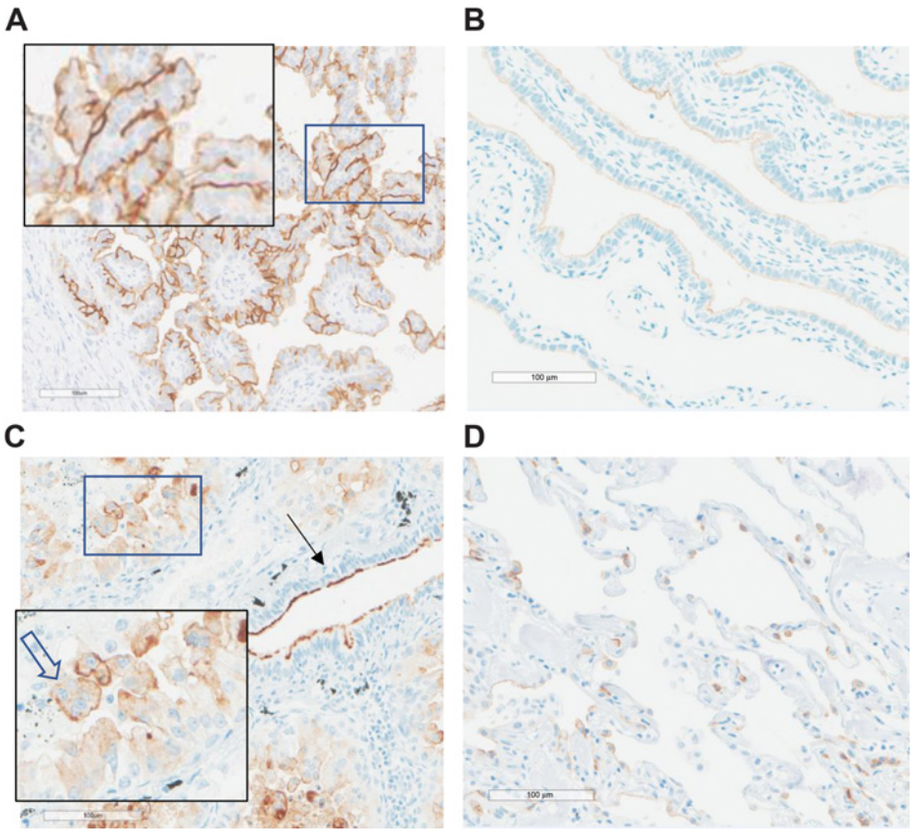

Figure 1.
NaPi2b expression in ovarian cancer (**A**), fallopian tube epithelium (**B**), normal bronchial epithelium (solid arrow) adjacent to NaPi2b-staining lung adenocarcinoma (open arrow; **C**), and type 2 pneumocytes in lung parenchyma (**D**). In the tumor images, insets are enlarged to show staining detail.

XMT-1536 shows target expression-dependent activity in a series of NSCLC adenocarcinoma PDXs

To confirm the results with OVCAR3 and extend the results to lung cancer, XMT-1536 was tested in a series of lung adenocarcinoma PDX models.

In model CTG-0178, XMT-1536 treatment did not result in tumor regressions when given at 3 mg/kg qwk ×3, but did cause significant delay of tumor growth, with a TGI of 67% ($P \leq 0.01$ vs. vehicle) at end of study, day 35. Treatment with the comparator, lifastuzumab-vedotin, or a nonbinding IgG1-Dolaflexin control ADC failed to cause tumor regression and did not lead to any significant growth delay (**Fig. 3B**).

In model CTG-0852, XMT-1536 achieved regressions at the 3 mg/kg qwk × 3 schedule, with 5 mice achieving PR, 1 CR, and 2 mice tumor free at the day 62 end of study. The nonbinding IgG1-Dolaflexin ADC did not induce tumor regression at the 3 mg/kg qwk × 3 schedule, but was associated with some tumor growth delay. Lifastuzumab-vedotin at 3 mg/kg was partially active, with 3/8 PR (**Fig. 3C**).

In model CTG -0860, XMT-1536 achieved PR in 2/7 mice at the 3 mg/kg qwk × 3 schedule, at day 60 end of study, with no responses seen in either the comparator or control group (**Fig. 3D**).

IHC was performed on representative vehicle blocks from each model and demonstrated the presence of NaPi2b target in each model.

XMT-1536 is highly active in a panel of ovarian adenocarcinoma PDXs

Twenty patient-derived ovarian/fallopian tube adenocarcinoma xenografts were evaluated for response to XMT-1536. These models were chosen without knowledge of NaPi2b expression, to mimic an unselected patient population. XMT-1536 induced at least 50% reduction in tumor volume relative to baseline in 10/20 (50%) models when administered at a dose of 3 mg/kg once weekly for 3 weeks (**Fig. 4A**). Responses were seen in both treatment-naïve and treatment-exposed tumor models (5/8 and 5/12, respectively).

The NaPi2b IHC assay was applied to a control block for each model and scored using an H-score algorithm. Tumors representative of low, moderate and high NaPi2b staining are shown in **Fig. 4B**. Amongst tumors with H-score ≥70, 10/13 models (76%) achieved 50% or greater reduction in tumor volume after XMT-1536 treatment, versus 0/7 models (0%) with H-score <70 (**Fig. 4C**).

Twenty human ovarian tumors were stained and scored with the NaPi2b IHC assay (**Fig. 4D**; Supplementary Table S1). The distribution of H-scores was comparable in these human ovarian tumors and the tested patient-derived xenograft models. Twelve of 20 (60%) human ovarian tumors evaluated for NaPi2b expression had an H-score ≥70. The human tumors showed a trend toward a bimodal distribution, with most tumors having an H-score of 100 or above or 50 or below, suggesting that the H-score threshold of 70 identified in the xenograft panel may represent discrimination of two different tumor populations based upon NaPi2b expression and XMT-1536 sensitivity.

The same IHC assay that was applied to staining human ovarian tumors was used on a panel of 20 human lung adenocarcinomas. Sixteen of 20 (80%) of tumors showed strong staining for NaPi2b (Supplementary Fig. S3).

Toxicology and PK studies

A tumor-bearing mouse biodistribution study demonstrated the specific targeting of XMT-1536 to NaPi2b expressing tumors. Maximum concentration of total AF-HPA in tumor tissue was observed at 96 hours after XMT-1536 administration, consistent with delayed penetration and target-dependent accumulation of the ADC in the

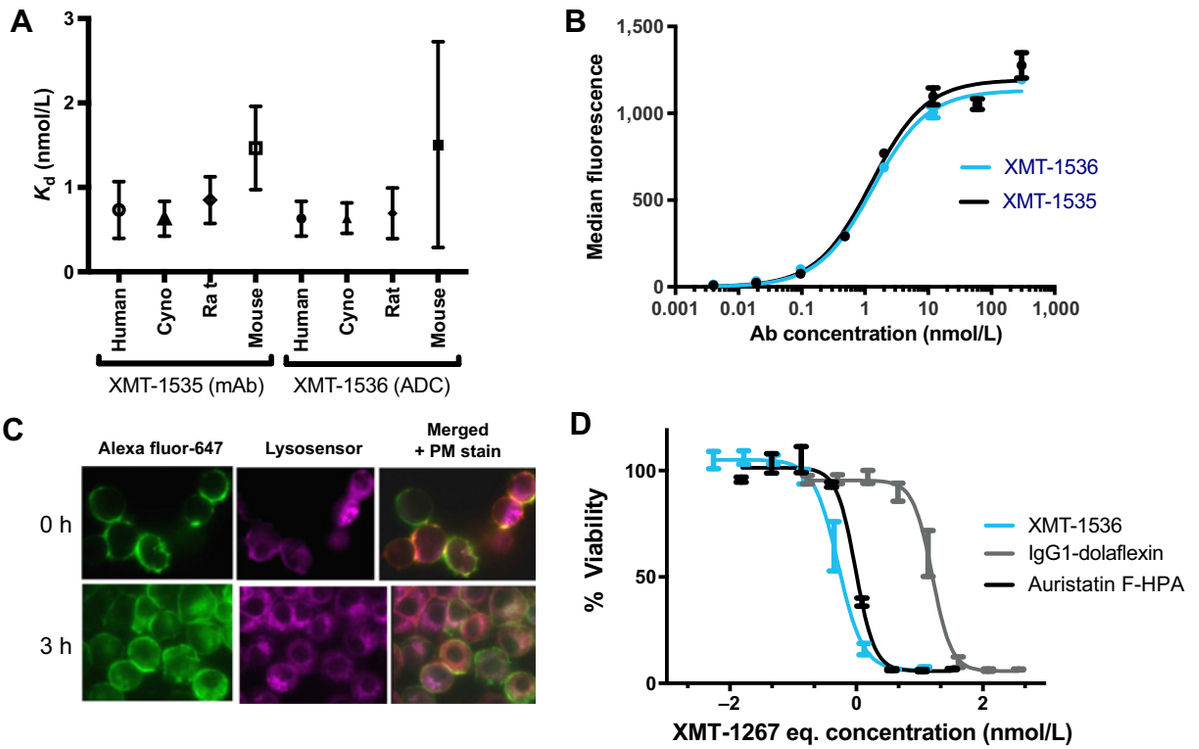

Figure 2.

In vitro characterization of XMT-1536. **A,** Affinity of XMT-1535 mAb and XMT-1536 ADC for NaPi2b peptide sequences from human, cynomolgus monkey, rat, and mouse. **B,** Binding of XMT-1535 and XMT-1536 to OVCAR3 ovarian cancer cells. **C,** Fluorescence microscopy demonstrates internalization of XMT-1535 mAb into OVCAR3 cells at 0 (top) and 3 hours (bottom) of incubation. **D,** *In vitro* cytotoxicity of XMT-1536 (blue line) in OVCAR3 ovarian cancer cells compared with IgG-Dolaflexin (gray line) and AF-HPA drug payload (black line). Doses expressed as concentration by payload (AF-HPA).

tumor tissue. Exposure to total AF-HPA, free AF-HPA, and free AF in other tissues (i.e., lung, liver, kidney, skeletal muscle, and spleen) was at least an order of magnitude less than that seen in tumor tissue. All analytes continued to be detectable in tumor tissue at 14 days (**Fig. 5**; Supplementary Fig. S4). NaPi2b target expression is conserved in mouse and mouse lung target tissue expression is shown in Supplementary Fig. S5.

Table 1. Cell-cycle effects of XMT-1536.

Treatment	Concentration (nmol/L)	Percentage of cells in G_2–M
None	0	34.3
XMT-1536	0.01	39.9
XMT-1536	0.05	45.4
XMT-1536	0.1	55
XMT-1536	0.5	73
XMT-1536	1	71.1
None	0	38.4
Bafilomycin A	0	33.6
XMT-1536	0.1	45.6
XMT-1536 + Bafilomycin A	0.1	31.8
XMT-1536	0.5	74.5
XMT-1536 + Bafilomycin A	0.5	37.4

Note: OVCAR3 cells were treated with XMT-1536 ranging from 0 to 1 nmol/L and in some cases 30 nmol/L Bafilomycin A for 24 hours. The amount of nuclear DNA in each cell was quantified in 5,000 cells for each treatment by a MACSQuant flow cytometer (Miltenyi Biotec) using propidium iodide. The percentage of arrested cells was determined by dividing the number of cells in G_2–M phase by the total number of cells and multiplying by 100.

XMT-1536 was evaluated in repeat dose toxicity studies in rat and cynomolgus monkey. The findings allowed us to establish the highest nonseverely toxic dose, used in determining the initial dose level in a phase I clinical study. Toxicokinetics were evaluated in rat and monkey. Total antibody, total AF-HPA, free AF-HPA, and free AF, were evaluated to characterize PK of XMT-1536 in the plasma. Exposure to each analyte was approximately dose-proportional in both species (**Fig. 6A**). Furthermore, there was no gender impact on PK in either species. In rats, the 3 mg/kg dose resulted in total AF-HPA payload $AUC_{0-\infty}$ of 251,000 hour/ng/mL in females and 278,000 hour/ng/mL in males. The exposure for total AF-HPA in monkeys after a 3 mg/kg dose was similar, with $AUC_{0-\infty}$ of 299,000 hour/ng/mL in females and 321,000 hour/ng/mL in males. In both species, the systemic maximum concentration of free AF-HPA and free AF after the 3 mg/kg XMT-1536 dose was less than 2 ng/mL with a T_{max} generally later for AF compared with AF-HPA (>72 vs. <24 hours, respectively; **Fig. 6A**). The exposures for rat, monkey, and tumor-bearing mouse are shown in **Fig. 6B**.

Tissue cross-reactivity

XMT-1536 used as a primary IHC reagent produced membrane and cytoplasmic staining in a variety of cell types. Human tissues with immunoreactivity included, but were not limited to, fallopian tube, kidney, bile duct epithelium, pulmonary pneumocytes and bronchial epithelium, ovarian surface epithelium; pancreatic ductal epithelium;

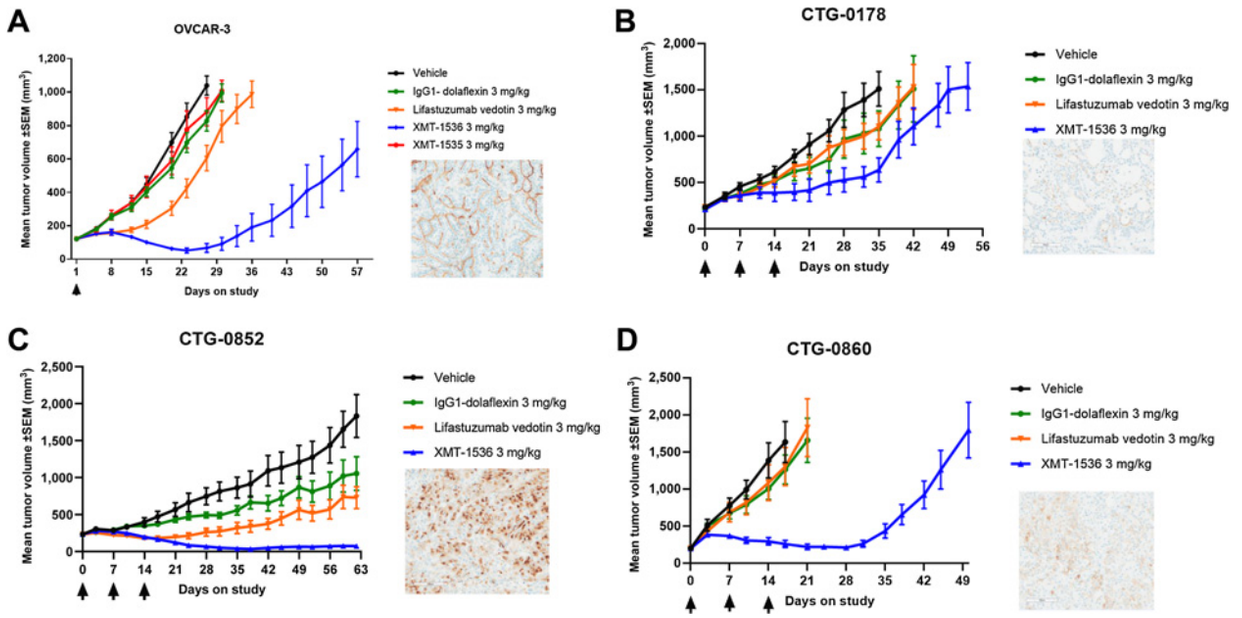

Figure 3.

A, XMT-1536 induced tumor regression in OVCAR3 xenograft models when administered at a single dose of 3 mg/kg. The control ADC IgG1-Dolaflexin was inactive, and the comparator lifastuzumab vedotin did not induce tumor regressions and achieved shorter tumor growth delay compared with XMT-1536. **B–D,** Three primary lung xenograft models showed antitumor activity following XMT-1536 dosed at 3 mg/kg qwk x 3 when compared with a control IgG-Dolaflexin or comparator lifastuzumab vedotin. Insets show IHC staining using an anti-NaPi2b antibody on representative formalin-fixed, paraffin-embedded blocks from mice not exposed to compound.

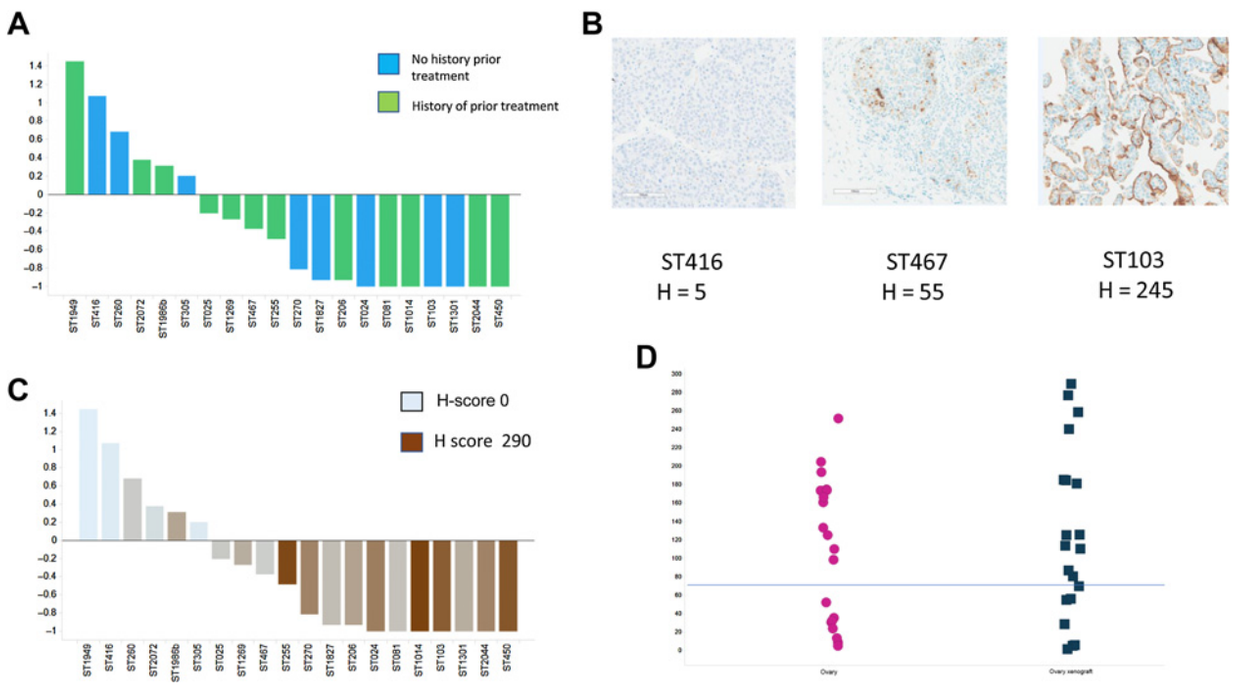

Figure 4.

Preclinical efficacy of XMT-1536 in a panel of epithelial ovarian and fallopian tube cancer PDXs. **A,** Waterfall plot of median best response from baseline for 20 ovarian PDX models, colored by history of prior treatment. **B,** Representative NaPi2b IHC from untreated xenografts showing low, medium, and high expression. **C,** Waterfall plot of median best response, shaded by IHC H-score. In this figure, the bars are colored from blue to brown to represent increasing deposition of brown DAB on a blue hematoxylin counterstained slide. Individual H scores are listed in Supplementary Table 1. **D,** IHC H-scores from ovarian tumors ($n = 20$) compared with IHC H-scores ($n = 20$) from the preclinical models run in this *in vivo* study.

Figure 5.

XMT-1536 administered to tumor-bearing mice, resulted in target dependent accumulation of the ADC in tumor. Concentrations of total AF-HPA, free AF-HPA, and free AF are shown in OVCAR3 xenograft tumors (circles, solid line) and lung tissue (triangles, dashed lines). Lung is considered to be a target organ for a NaPi2b ADC, but despite high levels of target expression, exposure in lung was at least an order of magnitude less than was seen in tumor.

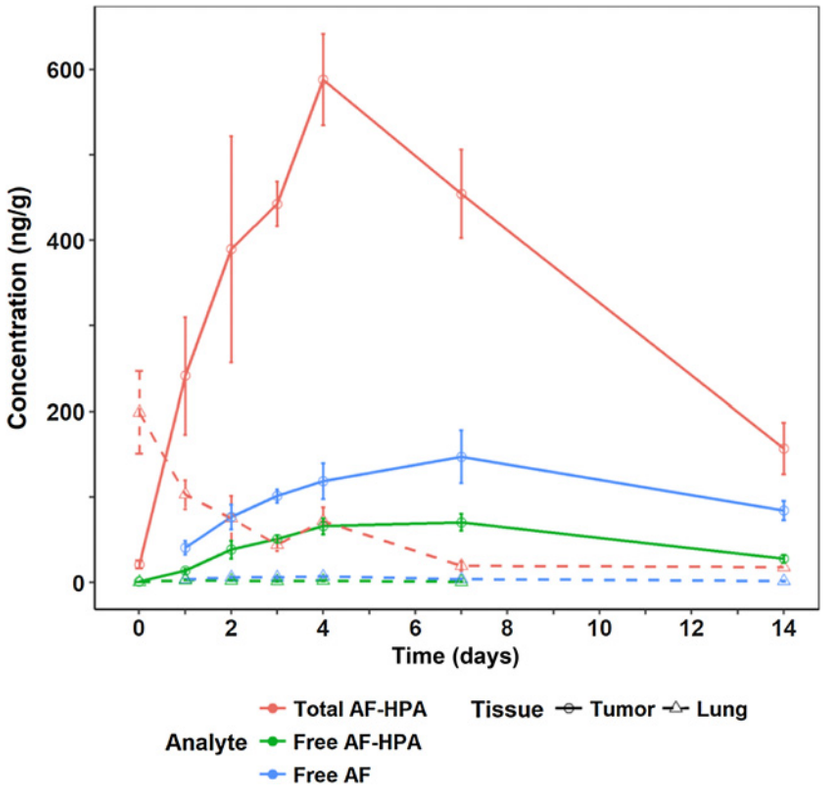

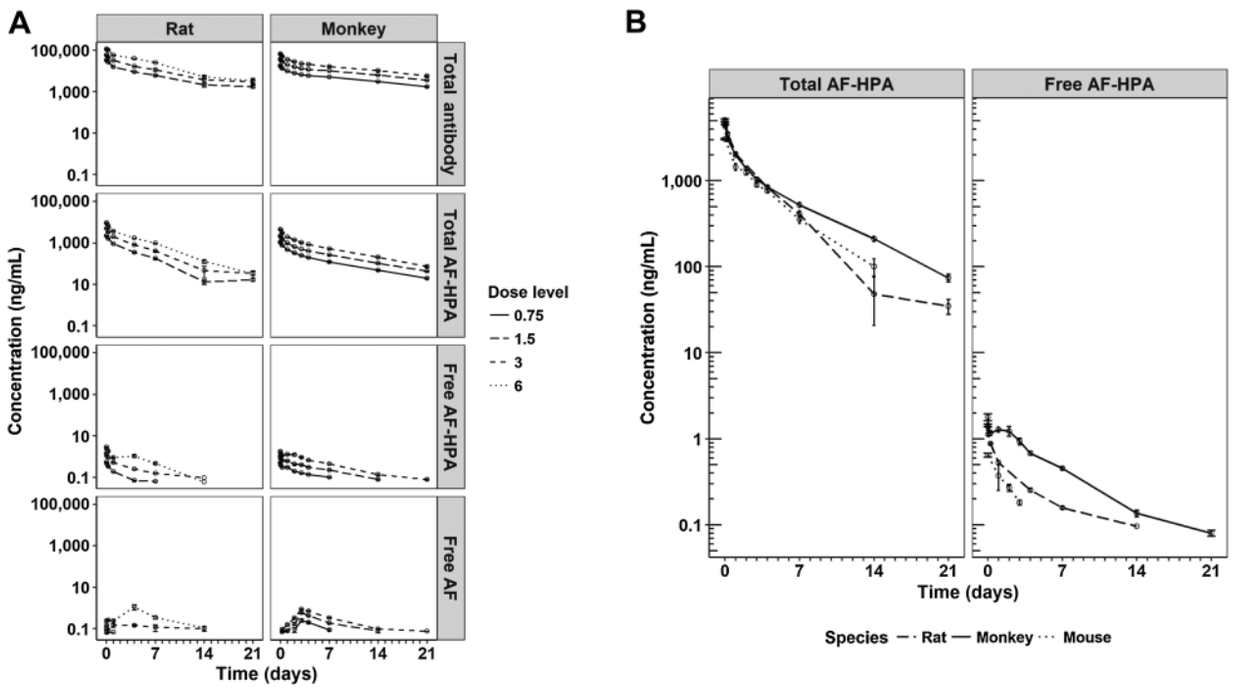

Figure 6.

A, Exposure of all analytes, including total antibody, total AF-HPA, free AF-HPA, and free AF, was dose proportional in both rat and cynomolgus monkey. **B,** Exposures for total AF-HPA and free AF-HPA in OVCAR3-bearing mice were lower than those in rat and monkey after a single 3 mg/kg dose of XMT-1536.

mesothelium; thyroid follicles; endocervix; and endometrium. Overall, there was concordance among the human, monkey, and rat tissue staining. One subtle difference in staining was the lower level of expression on the bronchial epithelium in rats compared with monkeys and humans although overall there was expression of NaPi2b in lung tissue for rats, monkeys, and humans. In the eye there was plasma membrane staining in human but not in rat or monkey. In the monkey, occasional weak immunoreactivity was seen in the eye epithelial cytoplasm.

Discussion

ADCs have shown promise in the treatment of cancer, but the identification of appropriate targets (especially for solid tumor ADCs) and the limitations of first-generation linker–payload platforms have remained challenges to achieving broader clinical success.

We, and others, (16) have demonstrated NaPi2b expression in NSCLC adenocarcinoma and epithelial ovarian cancer and in the presumed normal tissues of origin, type II pneumocytes and fallopian tube epithelium, respectively (28, 29). Our study uses a novel IHC reagent and the data is generally comparable to protein and RNA data expression data described by others. However, our IHC method was calibrated with outcome in a large series of primary xenograft models and this may allow us to predict levels of NaPi2b expression that will correspond to responsiveness to XMT-1536 in human tumors. XMT-1536 targets NaPi2b using the Dolaflexin platform. Consistent with the known mechanism of action of the auristatin class (30), XMT-1536 induced cell-cycle arrest in G_2–M that was dependent upon antigen-mediated ADC internalization and lysosomal processing. XMT-1536 was capable of inducing regressions in multiple PDX models of NSCLC adenocarcinoma and epithelial ovarian cancer, including durable complete regressions in several models.

Biodistribution studies in mice showed no antigen-dependent ADC accumulation in normal lung, a tissue with target expression, and substantially lower exposure to AF-HPA and AF in the lung compared with tumor. This difference between tumor and lung could be due to target accessibility, rate of antibody internalization, or other factors.

The pharmacokinetics of XMT-1536 were assessed in mice, rats, and monkeys after intravenous administration. PK analyses showed approximately dose proportional exposure of XMT-1536 in both rat and monkey. Systemic free AF-HPA and AF concentrations were several orders of magnitude lower than total AF-HPA in all animal species. In addition, specific tumor targeting of auristatin payload by XMT-1536 was illustrated in the mouse tissue distribution study. Overall, the PK characteristics of XMT-1536 are consistent with those of other ADCs in the clinic, despite the much higher DAR value of 10–15.

We postulated that a feature of a lineage-associated antigen target would be broad expression in tumors arising from a given cell lineage. We detected NaPi2b expression in many NSCLC adenocarcinoma and epithelial ovarian cancer cases using IHC, with an estimated 60% of ovarian cancer cases having NaPi2b-expression at a level associated with regressions in the PDX models. Notably, in both the NSCLC adenocarcinoma and ovarian cancer tumor panels evaluated here, there was an apparent bimodal distribution of NaPi2b H-scores, with a minority of tumors showing very low expression. These data suggest that NaPi2b IHC might be used to enrich for patient populations that respond to XMT-1536 therapy.

Despite recent advances in the treatment of non–small cell lung cancer and ovarian cancer, there remains a significant need for new therapies for patients with heavily pretreated disease, immunologically cold tumors (in NSCLC), or tumors with intact DNA repair mechanisms. On the basis of the data presented here, clinical investigation of XMT-1536 in these diseases and other NaPi2b-expressing tumors is warranted. XMT-1536 currently is being explored in early clinical studies of ovarian and lung adenocarcinoma. Clinical activity has been seen at doses of 20 mg/m^2 q4w and higher. At the MTD of 43 mg/m^2 q4w, severe toxicities such as neutropenia and neuropathy seen in other ADC studies have not been observed following treatment with XMT-1536 (31). Finally, the data presented here suggest that other solid tumor lineage antigens might be suitable as therapeutic targets for next-generation ADCs.

Authors' Disclosures

N.D. Bodyak reported other from Mersana Therapeutics outside the submitted work. R. Mosher reported personal fees and other from Mersana Therapeutics during the conduct of the study; in addition, R. Mosher had a patent for US 2019/0160181 pending. C. Bu reported other from Mersana outside the submitted work. D.R. Demady reported other from Mersana Therapeutics during the conduct of the study. M.J. DeVit reported personal fees from Mersana Therapeutics outside the submitted work. D.R. Gumerov reported personal fees from Mersana Therapeutics during the conduct of the study. W. Lee reported other from Mersana Therapeutics outside the submitted work. P.U. Park reported personal fees from Mersana Therapeutics during the conduct of the study; personal fees from Mersana Therapeutics outside the submitted work; in addition, P.U. Park had a patent for Mersana Therapeutics pending and issued. D.A. Bergstrom reported a patent for US2017/0266311 pending to Mersana Therapeutics and a patent for US2019/0160181 pending to Mersana Therapeutics. No disclosures were reported by the other authors.

Authors' Contributions

N.D. Bodyak: Conceptualization, supervision, investigation, methodology, writing–original draft. **R. Mosher:** Formal analysis, supervision, investigation, methodology, writing–original draft, writing–review and editing. **A.V. Yurkovetskiy:** Conceptualization, formal analysis, supervision, investigation, methodology, writing–original draft. **M. Yin:** Investigation, methodology. **C. Bu:** Investigation. **P.R. Conlon:** Investigation. **D.R. Demady:** Supervision, investigation. **M.J. DeVit:** Investigation. **D.R. Gumerov:** Investigation, methodology. **D. Xiao:** Investigation. **V.R. Gurijala:** Investigation. **W. Lee:** Investigation. **D. McGillicuddy:** Investigation. **P.U. Park:** Conceptualization, supervision, investigation. **L.L. Poling:** Investigation. **M. Protopopova:** Investigation. **L. Qin:** Investigation. **C.A. Stevenson:** Investigation. **E. Ter-Ovanesyan:** Investigation. **A. Uttard:** Investigation. **J. Xu:** Investigation. **L. Xu:** Investigation, methodology. **D.A. Bergstrom:** Conceptualization, formal analysis, supervision, writing–original draft. **T.B. Lowinger:** Conceptualization, formal analysis, supervision, validation, investigation, methodology, writing–original draft, writing–review and editing.

Acknowledgments

The authors wish to thank Charles River Laboratories, Champions Oncology, and START for their contributions to the *in vivo* work; QualTek Molecular Laboratories for their performance and interpretation of IHC assays; Frontage for sample analysis; Drs. Marc Damelin, Dorin Toader, and Radha Iyengar for contributions in preparation of this manuscript; and Jeffrey Zurita and Scott Collins for preparation of figures.

The costs of publication of this article were defrayed in part by the payment of page charges. This article must therefore be hereby marked *advertisement* in accordance with 18 U.S.C. Section 1734 solely to indicate this fact.

Received March 24, 2020; revised October 5, 2020; accepted February 1, 2021; published first March 15, 2021.

References

1. Beck A, Goetsch L, Dumontet C, Corvaia N. Strategies and challenges for the next generation of antibody-drug conjugates. Nat Rev Drug Discov 2017;16:315–37.
2. Lambert JM, Morris CQ. Antibody-drug conjugates (ADCs) for personalized treatment of solid tumors: a review. Adv Ther 2017;34:1015–35.
3. Deutsch YE, Tadmor T, Podack ER, Rosenblatt JD. CD30: an important new target in hematologic malignancies. Leuk Lymphoma 2011;52:1641–54.
4. van der Weyden CA, Pileri SA, Feldman AL, Whisstock J, Prince HM. Understanding CD30 biology and therapeutic targeting: a historical perspective providing insight into future directions. Blood Cancer J 2017;7:e603.
5. Gravanis I, Tzogani K, van Hennik P, de Graeff P, Schmitt P, Mueller-Berghaus J, et al. The European Medicines Agency Review of Brentuximab Vedotin (Adcetris) for the treatment of adult patients with relapsed or refractory CD30+ hodgkin lymphoma or systemic anaplastic large cell lymphoma: summary of the scientific assessment of the committee for medicinal products for human use. Oncologist 2016;21:102–9.
6. Younes A, Gopal AK, Smith SE, Ansell SM, Rosenblatt JD, Savage KJ, et al. Results of a pivotal phase II study of brentuximab vedotin for patients with relapsed or refractory Hodgkin's lymphoma. J Clin Oncol 2012;30:2183–9.
7. Uy N, Nadeau M, Stahl M, Zeidan AM. Inotuzumab ozogamicin in the treatment of relapsed/refractory acute B cell lymphoblastic leukemia. J Blood Med 2018;9:67–74.
8. Appelbaum FR, Bernstein ID. Gemtuzumab ozogamicin for acute myeloid leukemia. Blood 2017;130:2373–6.
9. Tilly H, Morschhauser F, Bartlett NL, Mehta A, Salles G, Haioun C, et al. Polatuzumab vedotin in combination with immunochemotherapy in patients with previously untreated diffuse large B-cell lymphoma: an open-label, non-randomised, phase 1b-2 study. Lancet Oncol 2019;20:998–1010.
10. Ogitani Y, Aida T, Hagihara K, Yamaguchi J, Ishii C, Harada N, et al. DS-8201a, a novel HER2-targeting ADC with a novel DNA Topoisomerase I inhibitor, demonstrates a promising antitumor efficacy with differentiation from T-DM1. Clin Cancer Res 2016;22:5097–108.
11. Rosenberg JE, O'Donnell PH, Balar AV, McGregor BA, Heath EI, Yu EY, et al. Pivotal trial of enfortumab vedotin in urothelial carcinoma after platinum and anti-programmed death 1/programmed death ligand 1 therapy. J Clin Oncol 2019;37:2592–600.
12. Bardia A, Mayer IA, Vahdat LT, Tolaney SM, Isakoff SJ, Diamond JR, et al. Sacituzumab govitecan-hziy in refractory metastatic triple-negative breast cancer. N Engl J Med 2019;380:741–51.
13. Cardillo TM, Govindan SV, Sharkey RM, Trisal P, Goldenberg DM. Humanized anti-Trop-2 IgG-SN-38 conjugate for effective treatment of diverse epithelial cancers: preclinical studies in human cancer xenograft models and monkeys. Clin Cancer Res 2011;17:3157–69.
14. Damelin M, Zhong W, Myers J, Sapra P. Evolving strategies for target selection for antibody-drug conjugates. Pharm Res 2015;32:3494–507.
15. Tolcher AW. Antibody drug conjugates: lessons from 20 years of clinical experience. Ann Oncol 2016;27:2168–72.
16. Lin K, Rubinfeld B, Zhang C, Firestein R, Harstad E, Roth L, et al. Preclinical development of an anti-NaPi2b (SLC34A2) antibody-drug conjugate as a therapeutic for non-small cell lung and ovarian cancers. Clin Cancer Res 2015;21:5139–50.
17. Corut A, Senyigit A, Ugur SA, Altin S, Ozcelik U, Calisir H, et al. Mutations in SLC34A2 cause pulmonary alveolar microlithiasis and are possibly associated with testicular microlithiasis. Am J Hum Genet 2006;79:650–6.
18. Banerjee S, Oza AM, Birrer MJ, Hamilton EP, Hasan J, Leary A, et al. Anti-NaPi2b antibody-drug conjugate lifastuzumab vedotin (DNIB0600A) compared with pegylated liposomal doxorubicin in patients with platinum-resistant ovarian cancer in a randomized, open-label, phase II study. Ann Oncol 2018;29:917–23.
19. Gerber DE, Infante JR, Gordon MS, Goldberg SB, Martin M, Felip E, et al. Phase Ia study of anti-NaPi2b antibody-drug conjugate lifastuzumab vedotin DNIB0600A in patients with non-small cell lung cancer and platinum-resistant ovarian cancer. Clin Cancer Res 2020;26:364–72.
20. Bodyak N, Yurkovetskiy A. Delivering more payload (High DAR ADCs). In: Damelin M, editor. Innovations for next-generation antibody-drug conjugates. Totowa, NJ: Humana Press; 2018.
21. Clardy SM, Yurkovetskiy A, Yin M, Gumerov D, Xu L, Ter-Ovanesyan E, et al. Unique pharmacological properties of dolaflexin-based ADCs: a controlled bystander effect [abstract]. In: Proceedings of the American Association for Cancer Research Annual Meeting 2018; 2018 Apr 14–18; Chicago, IL. Philadelphia (PA): AACR; 2018. Abstract nr 754.
22. Yurkovetskiy A, Bodyak N, Yin M, Thomas JD, Conlon P, Stevenson CA, et al. Dolaflexin: A novel antibody-drug conjugate platform featuring high drug loading and a controlled bystander effect, submitted.
23. Mattes MJ, Look K, Furukawa K, Pierce VK, Old LJ, Lewis JL Jr, et al. Mouse monoclonal antibodies to human epithelial differentiation antigens expressed on the surface of ovarian carcinoma ascites cells. Cancer Res 1987;47:6741–50.
24. Yin BW, Kiyamova R, Chua R, Caballero OL, Gout I, Gryshkova V, et al. Monoclonal antibody MX35 detects the membrane transporter NaPi2b (SLC34A2) in human carcinomas. Cancer Immun 2008;8:3.
25. Lindegren S, Andrade LN, Back T, Machado CM, Horta BB, Buchpiguel C, et al. Binding affinity, specificity and comparative biodistribution of the parental murine monoclonal antibody MX35 (Anti-NaPi2b) and its humanized version rebmab200. PLoS One 2015;10:e0126298.
26. Lopes dos Santos M, Yeda FP, Tsuruta LR, Horta BB, Pimenta AA Jr, Degaki TL, et al. Rebmab200, a humanized monoclonal antibody targeting the sodium phosphate transporter NaPi2b displays strong immune mediated cytotoxicity against cancer: a novel reagent for targeted antibody therapy of cancer. PLoS One 2013;8:e70332.
27. Bergstrom DA, Bodyak N, Lowinger TB, Park PU, Poling L, Yurkovetskiy A, inventors; Mersana Therapeutics, assignee. NaPi2b-targeted antibody-drug conjugates and methods of use thereof. US Patent Application 20170266311A1. 2017 Sep 21.
28. Erickson BK, Conner MG, Landen CN Jr. The role of the fallopian tube in the origin of ovarian cancer. Am J Obstet Gynecol 2013;209:409–14.
29. Xu X, Rock JR, Lu Y, Futtner C, Schwab B, Guinney J, et al. Evidence for type II cells as cells of origin of K-Ras-induced distal lung adenocarcinoma. Proc Natl Acad Sci U S A. 2012;109:4910–5.
30. Dumontet C, Jordan MA. Microtubule-binding agents: a dynamic field of cancer therapeutics. Nat Rev Drug Discov 2010;9:790–803.
31. Richardson DL, Barve MA, Strauss JF, Ulahannan SV, Moore KN, Hamilton EP, et al. Phase I expansion study of XMT-1536, a novel NaPi2b-targeting antibody-drug conjugate (ADC): Preliminary efficacy, safety, and biomarker results in patients with previously treated metastatic ovarian cancer (OC) or non-small cell lung cancer (NSCLC). J Clin Oncol 38:15s, 2020 (suppl; abstr 3549).